Photoexcitation of $n \simeq 305$ Rydberg states in the presence of an rf drive field

S. Yoshida,[1] C. O. Reinhold,[2,3,*] J. Burgdörfer,[1,3] S. Ye,[4] and F. B. Dunning[4]

[1]*Institute for Theoretical Physics, Vienna University of Technology, Vienna, Austria, EU*

[2]*Physics Division, Oak Ridge National Laboratory, Oak Ridge, Tennessee 37831-6372, USA*

[3]*Department of Physics, University of Tennessee, Knoxville, Tennessee 37996, USA*

[4]*Department of Physics and Astronomy and the Rice Quantum Institute, Rice University, Houston, Texas 77005-1892, USA*

(Received 22 June 2012; published 9 October 2012)

The response of highly excited potassium Rydberg states with $n \sim 305$ to a sinusoidal electric drive field in the radio frequency (100–300 MHz) regime is examined by photoexcitation from the 4*s* ground state using a uv probe beam. The drive field couples many Rydberg levels simultaneously and results in a coherent response that leads to a variety of multiphoton processes. The excitation spectra are analyzed within the framework of Floquet theory and reveal signatures of quantum optical phenomena such as electromagnetically induced transparency and Autler-Townes splitting seen with few-level systems.

DOI: 10.1103/PhysRevA.86.043415 PACS number(s): 32.80.Rm, 32.80.Qk, 42.50.Gy

I. INTRODUCTION

Very-high-n ($n \sim 305$) Rydberg atoms, which have diameters of $\sim$10 μm, provide a valuable laboratory in which to study the behavior of mesoscopic systems and, because they lie near the classical limit, furnish an ideal testing ground to study the bridge between classical and quantum dynamics. Indeed, wave packets (i.e., nonstationary spatially localized wave functions) have been engineered that behave much like a particle moving along a classical trajectory with little dispersion [1]. Such "coherent" behavior can be maintained for many hundreds of periods if the wave packet is acted upon by a periodic driving force which provides a source of coherence for the system. Such extended coherence is easiest to obtain when the frequency of the driving force is close to the classical Kepler orbital frequency [2–4]. Even weak fields of a few millivolts per centimeter can provide strong driving because the dipole interaction scales as $\sim n^2$. Furthermore, extremely dilute ensembles of high-n Rydberg atoms can act as a strongly interacting many-body system because atom-atom interactions also increase rapidly with n, for example, the van der Waals coefficient scales as $C_6 \sim n^{11}$ [5,6].

In the present work we investigate, in the single atom limit, the behavior of high n, $n \sim 305$, potassium Rydberg states when subject to sinusoidal radio-frequency (rf) drive fields with frequencies in the range $\sim$100–300 MHz that include the classical Kepler frequency of $n \sim 305$ states ($\sim$ 233 MHz) and the frequency separations between neighboring p and s or d states ($\sim$105–125 MHz). The rf field leads to strong coupling between different Rydberg levels. Their highly nonlinear response, theoretically described by Floquet states [7,8], is investigated by photoexcitation from the 4*s* ground state using a uv probe beam. Many studies of quantum optical phenomena in both single atoms and in strongly interacting systems have been undertaken using three-level excitation schemes of either the Λ type or the ladder type illustrated in Fig. 1(a) [9–15] and a variety of interesting phenomena such as electromagnetically induced transparency (EIT) and coherent population trapping (CPT) have been observed. Frequently in such measurements two optical fields of comparable frequency, $\omega_{1,2}$, are employed. In studies of Rydberg atom excitation [see Fig. 1(a)] the first field couples the atomic ground state $|g\rangle$ to a low-lying excited state $|e\rangle$ while the second couples this state to an isolated Rydberg level $|r\rangle$. We consider here a different scenario in which a "strong" rf field is used to couple many different Rydberg levels and the response to this driving is examined using a "weak" uv probe field that directly connects the ground state $|g\rangle$ to the manifold of perturbed Rydberg states. (Note that here the frequencies of the drive and probe fields, $\omega_{\rm rf}$ and $\omega_{\rm uv}$, respectively, are very different with $\omega_{\rm rf} \ll \omega_{\rm uv}$.) Measurements of the (uv) absorption probability reveal quantum-optical effects such as Autler-Townes splitting [7] and EIT [9] together with novel spectral features associated with nonlinear multiphoton processes. For example, suppression of resonant absorption resembling EIT reappears for strong off-resonant driving due to Bloch-Siegert shifts [16]. The experimental data are found to be in good agreement with Floquet theory and with numerical simulations using the time-dependent Schrödinger equation (TDSE) within a truncated state space.

II. EXPERIMENTAL SETUP

The present apparatus, shown in Fig. 2, is described in detail elsewhere [17]. Potassium atoms contained in a tightly collimated beam are subject to a sinusoidal field with frequencies $\omega_{\rm rf} \sim$ 100–300 MHz and amplitudes, $F_{\rm rf} \sim 1$ mV cm^{-1} generated using a 2 gigasamples/s arbitrary wave-form generator whose output is applied to a nearby electrode creating an electric field that oscillates in the z direction indicated in Fig. 2. (Note that this field differs from that associated with, say, a propagating microwave beam because the magnetic field component is absent.) Since the dipole transition matrix elements $\langle n\ell|z|(n \pm 1)(\ell \pm 1)\rangle$ scale as $\sim n^2$, this weak rf field leads to strong coupling within the manifold of high Rydberg states. The resulting perturbations are probed by the crossed (uv) output of an extracavity-doubled frequency-stabilized Rh6G dye laser (also polarized along the z axis) that is tuned to excite transitions to Rydberg levels with $n \sim 305$. Experiments are performed in a pulsed

*Present address: Oak Ridge Institute for Science and Education, Oak Ridge, TN 37831, USA.

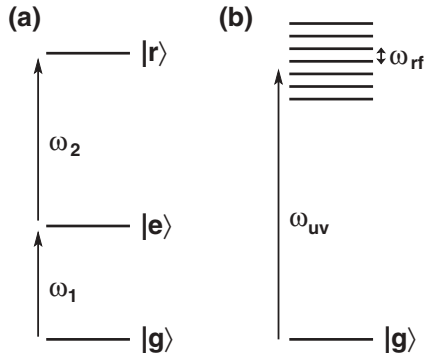

FIG. 1. Comparison between the standard three-level ladder scheme for coherent excitation of Rydberg levels utilizing two optical transitions with frequencies $\omega_{1,2}$ (a) and the coherent excitation of a multilevel Rydberg atom through rf driving that is probed using a uv laser pulse (b).

mode. A periodic train of concurrent rf and uv pulses, each $\sim$2 μs long, is applied with a pulse repetition frequency of $\sim$20 kHz. The number of Rydberg atoms created ($\ll$1 per laser pulse) is determined using selective field ionization for which purpose a slowly rising electric field (rise time $\sim$1 μs) is generated in the experimental volume by applying a positive voltage ramp to the lower electrode. Product electrons are accelerated out of the interaction region and are detected by a particle multiplier. The experimentally observed signal is proportional to the imaginary, i.e., absorptive, part of the linear susceptibility, $\mathrm{Im}\chi(\omega_{\mathrm{uv}};\omega_{\mathrm{rf}},F_{\mathrm{rf}})$, at uv frequencies and probes the nonlinear response of the Rydberg atoms to the rf field. The dispersive part of the linear response, $\mathrm{Re}\chi(\omega_{\mathrm{uv}};\omega_{\mathrm{rf}},F_{\mathrm{rf}})$, can be determined using the Kramers-Kronig relations [18,19].

Because of the splitting ($\sim$461 MHz) of the $F=1$ and $F=2$ ground hyperfine states in potassium, photoexcitation leads to the generation of two interleaved Rydberg series, one originating from each of the ground states, which complicates the excitation spectrum. However, in certain regions of the spectrum features associated with excitation from each hyperfine level overlap. Here we focus on the region near $n\sim 305$ where the ground-state hyperfine splitting matches the $\Delta n=2$ spacing between Rydberg manifolds and, consequently, the np and $(n-2)p$ states overlap. Working in this regime simplifies the excitation spectra (and hence their analysis) because, as illustrated in the energy diagram in Fig. 2, at very high n the spacing between Rydberg levels varies only slowly with n and the two superposed n series exhibit very similar behaviors. To further check this, measurements were undertaken with the laser tuned to excite transitions to $n\sim 320$ states where two well-resolved Rydberg series are observed. Application of the rf drive field resulted in changes in each separate Rydberg series similar to those seen in the superposed spectra at $n\sim 305$.

III. FLOQUET THEORY

The photoexcitation of potassium by a laser field $F_{\mathrm{uv}}\sin(\omega_{\mathrm{uv}}t)$ in the presence of an rf field $F_{\mathrm{rf}}\sin(\omega_{\mathrm{rf}}t)$ can be described by the Hamiltonian

$$H=\frac{p^2}{2}+V(r)+zF(t), \tag{1}$$

where $V(r)$ is a one-electron model potential (atomic units are used throughout unless otherwise noted). The fields

$$F(t)=F_{\mathrm{uv}}\sin(\omega_{\mathrm{uv}}t)+F_{\mathrm{rf}}\sin(\omega_{\mathrm{rf}}t) \tag{2}$$

are taken to be linearly polarized along the z axis. Though the laser field amplitude ($\sim$10–100 V cm^{-1}) is a factor of 10^4 larger than the typical rf field strengths employed, the dipole matrix elements between ground and Rydberg states are much smaller than those between neighboring Rydberg states (for $n\sim n'\sim 300$, $\langle 4s|z|n\ell\rangle\simeq 10^{-4}$ whereas $\langle n\ell|z|n'\ell'\rangle\simeq 10^4$). The rf field thus plays the role of a strong pump field while the uv laser field provides a weak probe field.

The Floquet states $|\phi_k^F(t)\rangle$ resulting from dressing by the rf field satisfy the eigenvalue equation

$$U(t+T_{\mathrm{rf}},t)\left|\phi_k^F(t)\right\rangle=e^{i\mathcal{E}_kT_{\mathrm{rf}}}\left|\phi_k^F(t)\right\rangle, \tag{3}$$

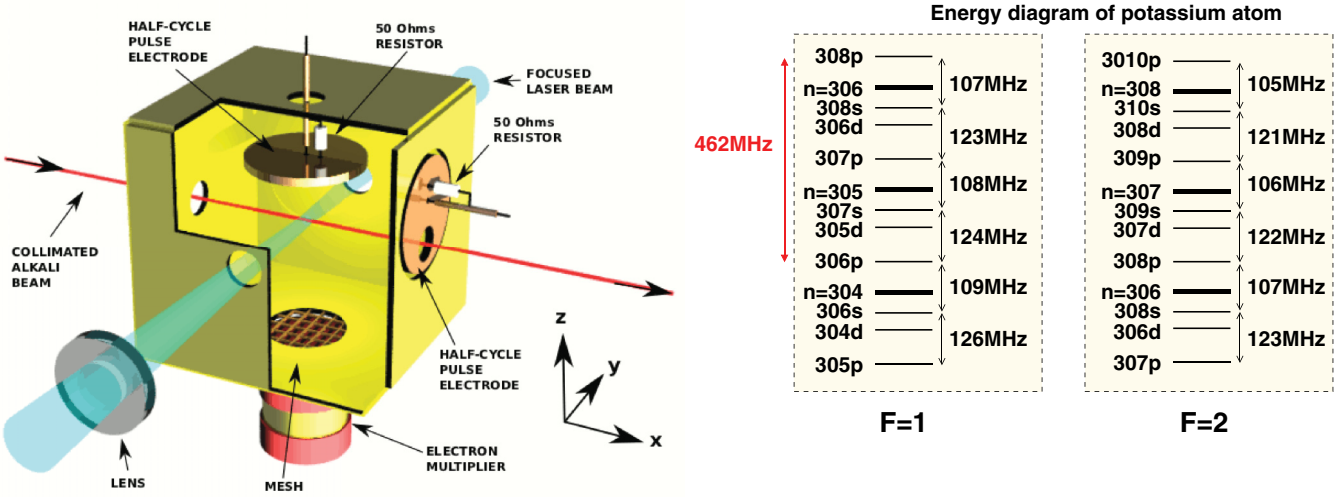

FIG. 2. (Color online) Schematic diagram of the apparatus. The inset shows a partial term diagram for potassium depicting the two Rydberg series of interest here that originate on the $F=1$ and $F=2$ ground hyperfine states. The arrows indicate the energy separations between neighboring s and p levels.

where $U(t+T_{\rm rf},t)$ ($T_{\rm rf}=2\pi/\omega_{\rm rf}$) is the period-1 evolution operator for the Hamiltonian

$$H=\frac{p^2}{2}+V(r)+zF_{\rm rf}\sin(\omega_{\rm rf}t). \tag{4}$$

As the time evolution operator is a unitary operator, the quasienergy of the Floquet state, $\mathcal{E}_k$, is real. We expand the Floquet states in terms of the field-free states, $|\phi_{n,\ell}\rangle$, of potassium,

$$\left|\phi_k^F(t)\right\rangle=\sum_{n,\ell}c_{n,\ell}(t)|\phi_{n,\ell}\rangle. \tag{5}$$

While the Floquet state accumulates the phase $e^{-i\mathcal{E}_kT_{\rm rf}}$ per period, the remainder of the wave function is strictly periodic due to the periodicity of the Hamiltonian. Allowing for a Fourier series expansion of the dressed state,

$$\left|\phi_k^F(t)\right\rangle=e^{-i\mathcal{E}_kt}\sum_{n,\ell}\sum_N\tilde{c}_{n,l}(N)e^{-iN\omega_{\rm rf}t}|\phi_{n,\ell}\rangle, \tag{6}$$

the photoexcitation rate and, hence, $\mathrm{Im}\chi$, is proportional to the dipole oscillator strength from the $4s$ ground state [7],

$$\begin{aligned}\mathrm{Im}\chi(\omega_{\rm uv};\omega_{\rm rf},F_{\rm rf})&\propto\mu(\mathcal{E}_k,N)\\&=\left|\sum_n\tilde{c}_{n,\ell=1}(N)\langle\phi_{n,\ell=1}|z|\phi_{4,0}\rangle\right|^2,\end{aligned} \tag{7}$$

where only the projection onto the p state ($\ell=1$) of the dressed Rydberg state contributes. For resonant absorption, the uv laser frequency and $\omega_{\rm rf}$ must satisfy

$$\omega_{\rm uv}=\mathcal{E}_k+N\omega_{\rm rf}, \tag{8}$$

where N is the photon number of the corresponding quasienergy band $(\mathcal{E}_k,N)$. We calculate the excitation spectrum numerically by representing the Hamiltonian [Eq. (1)] in matrix form using a truncated basis ($n_{\rm min}\leqslant n\leqslant n_{\rm max},\ell\leqslant\ell_{\rm max},m=0$). The eigenenergies of the Hamiltonian in the field-free basis are evaluated using the experimentally measured values of the quantum defect [20] rather than deriving them from a model potential $V(r)$. The dipole matrix elements (including corrections due to the quantum defects) are evaluated semiclassically [21,22]. The period-1 evolution matrix [Eq. (3)] is derived from the Hamiltonian using the split-operator method and the quasienergies $\mathcal{E}_k$ are obtained by numerically diagonalizing the matrix. The evolution of the corresponding eigenstates is calculated by solving the TDSE. The expansion coefficients $c_{n,\ell}(t)$ are expanded in a Fourier series to obtain the oscillator strengths. The resulting calculated spectra are convoluted with a Gaussian distribution to mimic the Doppler broadening ($\Delta\sim15$ MHz) present in the measurements. The validity of the approach discussed above was confirmed by comparison with predictions made by directly solving the TDSE including both the ground state and the Rydberg levels as well as the two fields.

A. Harmonic oscillator model for potassium

Some of the complex features present in $\mathrm{Im}\chi$ for the "strong" rf driving discussed below can be analyzed with the help of a simplified three-dimensional (3D) spherical harmonic oscillator model. Key to this is the fact that, for a fixed value of ℓ, the n levels are to a good approximation equispaced and, moreover, that the quantum defects in potassium are such that the p levels lie approximately midway between the neighboring s and d levels. Consequently, the spectrum resembles that of a 3D oscillator with $\omega_{\rm osc}\simeq E_{n,\ell=1}-E_{n,\ell=0}\simeq E_{n+1,\ell=0}-E_{n,\ell=1}$. To set up a minimal model of a coherently excited multistate Rydberg atom three levels are required, for example ($306s$, $306p$, $307s$) or ($306p$, $307s$, $307p$). The corresponding model Hamiltonian $H_{\rm HO}$ in the product Hilbert space $|n,N\rangle$ for a harmonic oscillator with quantum number n and rf-photon space with photon number N becomes in the rotating wave approximation (RWA) [23]

$$H_{\rm HO}=\begin{pmatrix}(n-1)\,\omega_{\rm osc}+(N+1)\omega_{\rm rf} & -idF_{\rm rf}/2 & 0\\ idF_{\rm rf}/2 & n\omega_{\rm osc}+N\omega_{\rm rf} & -idF_{\rm rf}/2\\ 0 & idF_{\rm rf}/2 & (n+1)\,\omega_{\rm osc}+(N-1)\omega_{\rm rf}\end{pmatrix}, \tag{9}$$

where d is the dipole transition matrix element. Since the model is designed to approximate driven Rydberg atoms with $n\sim305$, the dipole transition matrix elements are assumed to be equal, $\langle n-1,N+1|d|n,N\rangle\simeq\langle n,N|d|n+1,N-1\rangle$. The Floquet eigenvalues of Eq. (9) are

$$\begin{aligned}\mathcal{E}_{1,2}&=n\omega_{\rm osc}+N\omega_{\rm rf}\pm\sqrt{\delta^2+d^2F_{\rm rf}^2/2},\\ \mathcal{E}_3&=n\omega_{\rm osc}+N\omega_{\rm rf},\end{aligned} \tag{10}$$

with the detuning $\delta=\omega_{\rm osc}-\omega_{\rm rf}$. For off-resonant driving ($|\delta|\gg|dF_{\rm rf}|$) the unperturbed energies (diagonal elements of the Hamilton matrix [Eq. (9)]) are nondegenerate. With increasing perturbation the two outer states $\mathcal{E}_{1,2}$ are repelled by the center state whose quasienergy $\mathcal{E}_3$ remains independent of $|dF_{\rm rf}|$. For weak perturbations the repulsion of the outer states is quadratic in $F_{\rm rf}$,

$$\mathcal{E}_{1,2}\simeq n\omega_{\rm osc}+N\omega_{\rm rf}\pm\delta\left(1+\frac{d^2F_{\rm rf}^2}{4\delta^2}\right). \tag{11}$$

On the other hand, for resonant driving ($|\delta|\ll|dF_{\rm rf}|$), the threefold degeneracy of the unperturbed states in the limit $\delta\to0$ is broken and the quasienergies separate linearly in $F_{\rm rf}$ from each other,

$$\mathcal{E}_{1,2}\simeq n\omega_{\rm osc}+N\omega_{\rm rf}\pm\frac{1}{\sqrt{2}}dF_{\rm rf}\left(1+\frac{\delta^2}{d^2F_{\rm rf}^2}\right). \tag{12}$$

The center state is given in terms of the product state $|n,N\rangle$ by

$$|\phi_3^F\rangle = \frac{1}{\sqrt{\delta^2 + 2d^2F_{\rm rf}^2}}(dF_{\rm rf}|n-1,N+1\rangle + 2i\delta|n,N\rangle + dF_{\rm rf}|n+1,N-1\rangle). \quad (13)$$

In the off-resonant limit ($|\delta| \gg |dF_{\rm rf}|$) Eq. (13) converges to the uncoupled center state $|n,N\rangle$ while in the resonant limit ($|\delta| \ll |dF_{\rm rf}|$) $|\phi_3^F\rangle$ converges to a coherent superposition of the two unperturbed states $|n-1,N+1\rangle$ and $|n+1,N-1\rangle$. The model Hamiltonian [Eq. (9)] can be applied to both the case where the unperturbed center state $|n,N\rangle$ is a p state, (i.e., $|n-1\rangle = |306s\rangle$, $|n\rangle = |306p\rangle$, $|n+1\rangle = |307s\rangle$) and where the center state is of s character (i.e., $|n-1\rangle = |306p\rangle$, $|n\rangle = |307s\rangle$, $|n+1\rangle = |307p\rangle$). However, the linear response, $\mathrm{Im}\chi$, as probed by the uv laser, for these two three-state manifolds is dramatically different.

B. Manifold with central p state

We explore now the application of the three-level harmonic oscillator model outlined above to a three-level Rydberg "atom" ($306s$, $306p$, $307s$) centered on the p state. Figure 3 compares the quasienergy spectrum obtained analytically using the harmonic oscillator model [Eq. (10)] and drive frequencies $\omega_{\rm rf} = 233$ and 116 MHz [Figs. 3(a) and 3(d)] with the simulated excitation spectra, i.e., $\mathrm{Im}\chi(\omega_{\rm uv};\omega_{\rm rf},F_{\rm rf})$, obtained for the three-state Rydberg manifold using the realistic values for energy spectrum and dipole matrix elements both with and without invoking the rotating wave approximation (RWA). For these comparisons, the parameters for the harmonic oscillator model are chosen as $\omega_{\rm osc} = (E_{307s} - E_{306s})/2$ and $d = (\langle\phi_{306s}|z|\phi_{306p}\rangle + \langle\phi_{306p}|z|\phi_{307s}\rangle)/2$. When the frequency of the drive field ($\omega_{\rm rf} = 233$ MHz) is far off resonance relative to the transition between the $306s$ and $306p$ levels (~109 MHz) and between the $306p$ and $307s$ levels (~124 MHz), the two outermost Floquet states (which are asymptotically connected to the s states in the weak-field limit) initially suffer quadratic energy shifts as the drive field is increased while the Floquet state associated with the unperturbed $306p$ state does not change in energy. As is apparent from Figs. 3(b) and 3(c), little excitation of the outermost Floquet states occurs at small drive fields because of their dominant s-like character. As the drive field increases these states acquire more p character and their excitation becomes more probable. For small to intermediate drive fields, the analytic harmonic oscillator model predicts the quasienergy spectrum of the absorption peaks quite well. Under strong-field driving ($F_{\rm rf} \gtrsim 5$ mV cm^{-1}), however, novel features appear that signify the breakdown of the RWA. The counter-rotating component of the drive field shifts the unperturbed energy levels, an effect known as the Bloch-Siegert shift [16] [this shift can be estimated by substituting $\delta = \omega_{\rm osc} + \omega_{\rm rf}$ in Eq. (10)]. Remarkably, for strong far-off resonant driving [Fig. 3(c)] the Floquet state associated with the unperturbed $306p$ state becomes transparent to laser excitation leading to electromagnetically induced transparency

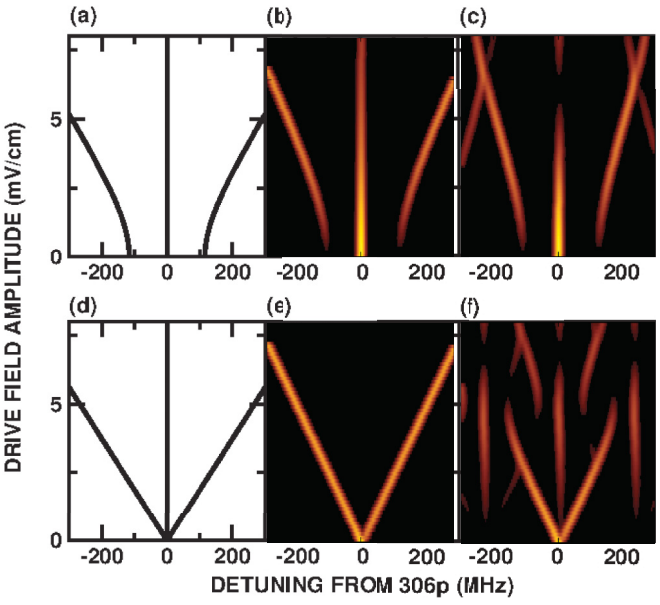

FIG. 3. (Color online) Floquet energies (a),(d) of the three-level driven harmonic oscillator [Eq. (9)] and excitation spectra (b),(c),(e),(f) of the three-level Rydberg atom ($306s$, $306p$, $307s$) driven by an rf field. The drive frequency is $\omega_{\rm rf} = 233$ MHz in (a)–(c) and 116 MHz in (d)–(f). The excitation strengths $\mathrm{Im}\chi$ of the Floquet states are estimated as $\mu(\mathcal{E}_k,N)$ [Eq. (6)] when the laser is tuned to the frequency $\mathcal{E}_k + N\omega_{\rm rf}$. The spectra are summed over all Floquet states and photon numbers N and convolved with a Gaussian to match with Doppler broadening ($\Delta \sim 15$ MHz) seen experimentally. The laser frequency resonant with excitation of the $306p$ state is defined as zero detuning. Excitation strengths calculated both with (b),(e), and without (c),(f) use of the RWA are included.

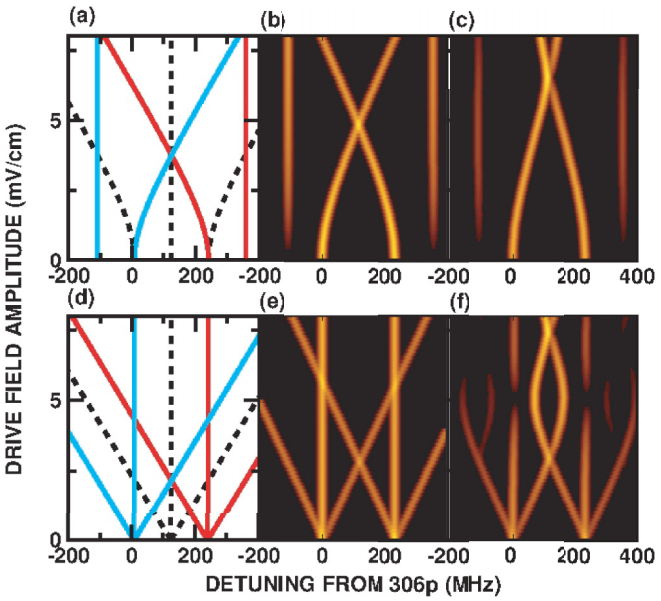

FIG. 4. (Color online) Floquet energies (a),(d) of the three-level driven harmonic oscillator [Eq. (9)] and excitation spectra (b),(c),(e),(f) of the three-level Rydberg atom ($306p$, $307s$, $307p$) driven by an rf field. The driving frequency is $\omega_{\rm rf} = 233$ MHz in (a)–(c) and 116 MHz in (d)–(f). In (a),(d) the dashed lines correspond to the Floquet energies $\mathcal{E}_i$ ($i = 1,2,3$) in Eq. (10) with $N = 0$, the red (dark gray) lines with $N = 1$, and the light blue (light gray) lines with $N = -1$. The excitation strengths are calculated and arranged as in Fig. 3.

(EIT). A different response emerges for near-resonant driving ($\omega_{\rm rf} = 116$ MHz). The three-level system is degenerate in the limit $F_{\rm rf} \to 0$. The quasienergy spectrum splits linearly with increasing drive field, an effect termed Autler-Townes splitting [7]. At low-to-intermediate values of $F_{\rm rf}$ the Floquet state associated with zero detuning is transparent to $\omega_{\rm uv}$ excitation. This can be readily understood using the simple harmonic oscillator model [Eq. (9)] and results because, in this limit, the state $|\phi_3^F\rangle$ is a superposition of two adjacent s states and therefore not optically accessible from the $4s$ ground state. However, for strong driving [Fig. 3(f)] the "zero-detuned" Floquet state becomes accessible because the counter-rotating field component destroys the EIT.

C. Manifold with central s state

As evident from Fig. 4(a), a dramatically different excitation spectrum emerges for a three-level Rydberg "atom" ($306p$, $307s$, $307p$) centered on an s state. For both off-resonant [Fig. 4(a)] and near-resonant driving [Fig. 4(d)] the quasienergies (dashed lines) agree with those in Figs. 3(a) and 3(d). However, the excitation spectra exhibit an entirely different behavior. The unperturbed $307s$ state is not directly accessible from the ground state by single-photon absorption. Transitions to this state must be accompanied by absorption or emission of an rf photon. Therefore, excitation is observed at Floquet energies that are shifted by $+\omega_{\rm rf}$ [red (solid black) lines] or $-\omega_{\rm rf}$ [light blue (gray) lines] relative to those for transitions that do not involve rf photons. For driving far off resonance the two dominant excitation peaks stem from the unperturbed $306p$ and $307p$ states. However, with increasing rf field strength, the absorption and emission of rf photons starts to become important resulting in the appearance of excitation at energies corresponding to $E_{307s} \pm \omega_{\rm rf}$. The Floquet energies of these states are independent of the strength of the perturbation, but the absorption, $\mathrm{Im}\chi$, depends markedly on whether or not the RWA is invoked. The two dominant p states, coupled with the $\omega_{\rm rf}$-shifted $307s$ state, form optically active Floquet states that exhibit quadratic energy shifts. However, as seen in Fig. 4(d), driving near resonance yields linear energy shifts. EIT is absent for weak drive fields because the corresponding Floquet state is a superposition of two p states and is optically accessible. For drive field strengths above $\sim$5 mV cm^{-1} the counter-rotating field brings the system out of the resonance and the energy shifts become quadratic in $F_{\rm rf}$. Because the multilevel excitation spectra involve different numbers of rf photons and because the energy levels belonging to different photon numbers are not coupled, their Floquet levels can cross.

IV. COMPARISON BETWEEN SIMULATED AND MEASURED SPECTRA

While the three-level Rydberg systems and the analytic harmonic oscillator model provide qualitative insights into the behavior of Rydberg atoms under rf driving, quantitative

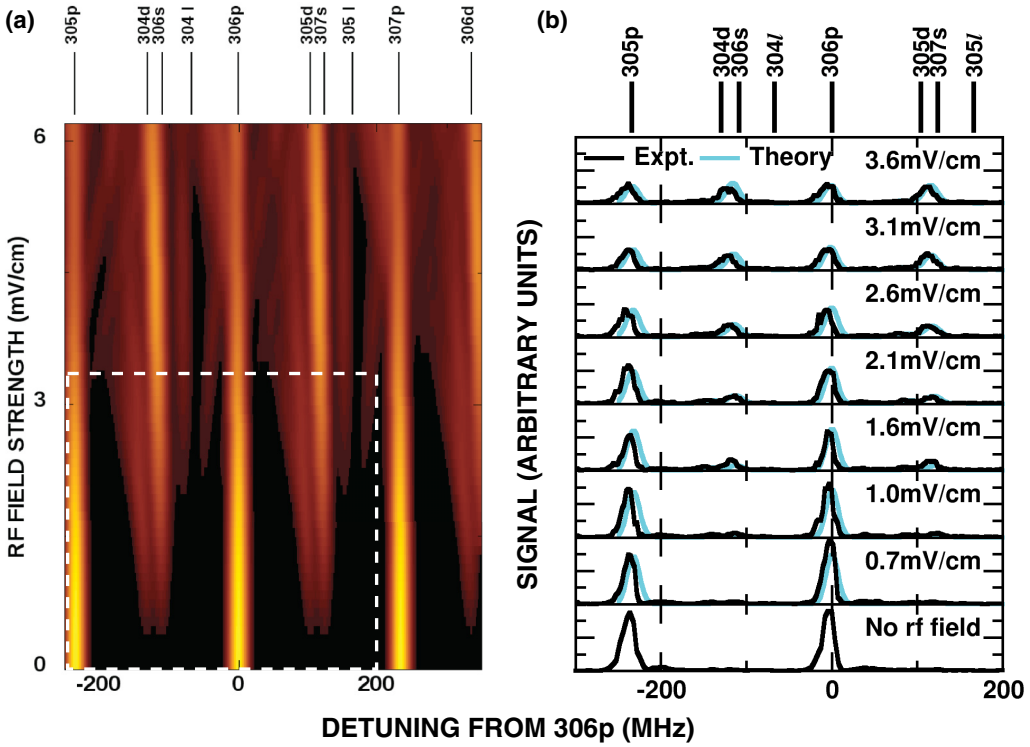

FIG. 5. (Color online) Evolution of the photoexcitation spectrum near $n \sim 305$ as a function of rf drive field amplitude for a drive frequency $\omega_{\rm rf} = 233$ MHz. (a) Excitation strengths [Eq. (14)] derived from the expansion coefficients $\mu(\mathcal{E}_k, N)$ calculated within the finite basis $284 \leqslant n \leqslant 324$, $0 \leqslant \ell \leqslant 10$, and $m = 0$. (b) Comparison of experimental data (black lines) with simulated spectra [blue (gray) lines] obtained by making cuts through (a) at selected field strengths within the white dashed rectangle. The positions of the zero-field resonances are indicated.

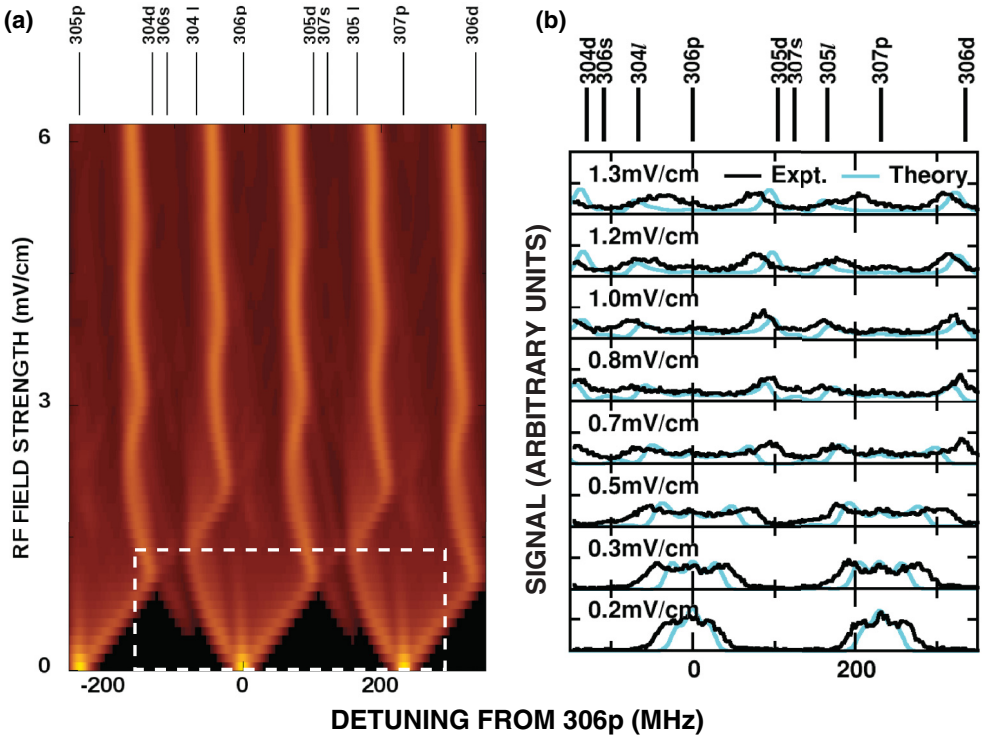

FIG. 6. (Color online) Evolution of the photoexcitation spectrum near $n \sim 305$ as a function of rf drive field amplitude for a drive frequency $\omega_{\rm rf} = 116$ MHz. The excitation strengths are calculated, and the figure is arranged, as in Fig. 5.

comparisons with experiment require the inclusion of many n and l states to allow for multi-(rf) photon emission and absorption. The calculations presented here were undertaken using a finite basis with $284 \leqslant n \leqslant 324$, $0 \leqslant \ell \leqslant 10$, and $m = 0$.

Excitation probabilities for off-resonant driving ($\omega_{\rm rf} = 233$ MHz) and for near-resonant driving ($\omega_{\rm rf} = 116$ MHz) are shown in Figs. 5 and 6, respectively, as a function of rf field strength and compared with experimental data. For low-to-intermediate strengths of an off-resonant drive field (Fig. 5) the positions of the dominant absorption peaks remain nearly constant in qualitative agreement with the harmonic oscillator model (Fig. 3). (In the multilevel system the "collective" repulsion from levels both below and above averages to near zero thereby leaving their positions essentially unchanged.) With increasing $F_{\rm rf}$ both ns and $(n-2)d$ states become accessible. The strength $S_{n\ell}$ of the excitation of these states can be quantified by the integral

$$S_{n\ell} \propto \int_{\delta_{n\ell}-\Delta}^{\delta_{n\ell}+\Delta} d\omega_{\rm uv}\, {\rm Im}\chi(\omega_{\rm uv};\omega_{\rm rf},F_{\rm rf}) \qquad (14)$$

over the linewidth (Fig. 5). For the s and d components, $S_{n,\ell=0,2}$ increases quadratically with $F_{\rm rf}$ consistent with Eq. (13). As illustrated in Fig. 7, the growth of the features in the measured spectra associated with the excitation of s and d states [$S_{307s} + S_{305d}$ in (a) and $S_{306s} + S_{304d}$ in (b)] is in good agreement with that of the excitation strengths predicted by Eq. (14). The dominant contribution of s states to the s,d features was confirmed by rotating the plane of polarization of the uv laser approximately 90° using a (nearly) half wave plate. With such rotation only the creation of product states with $m = \pm 1$ is allowed, discriminating against creation of final ns states. Although a measure of elliptical polarization remained in the laser beam after insertion of the half wave plate, its presence reduced the size of the multiphoton features by ~70% confirming the dominance of ns final states. The symmetry of the excitation branches relative to the dominant np state seen for the harmonic oscillator model is broken in the multilevel Rydberg atom and one nearly linearly shifted branch with a negative slope dominates. For strong driving fields $F_{\rm rf} \gtrsim 5$ mV cm^{-1} the excitation of p states becomes suppressed, which is a remnant of the EIT induced by the Bloch-Siegert shift. For near-resonant driving ($\omega_{\rm rf} = 116$ MHz) (Fig. 6) the excitation peaks associated with the p states split and form two (or three) peaks whose spacing

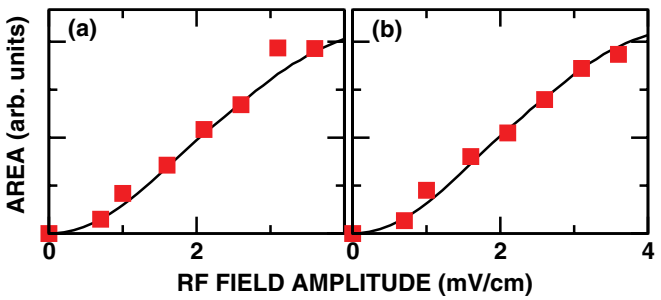

FIG. 7. (Color online) Growth of the features seen in Fig. 5(b) associated with excitation of (a) $304d$, $306s$ and (b) $305d$, $307s$ states as a function of rf drive field amplitude: ■, experimental data; ——, integrated excitation strengths [Eq. (14)]. The integration ranges are (a) $\delta_{305d} - 20$ MHz $< \omega_{\rm uv} < \delta_{307s} + 20$ MHz and (b) $\delta_{304d} - 20$ MHz $< \omega_{\rm uv} < \delta_{306s} + 20$ MHz.

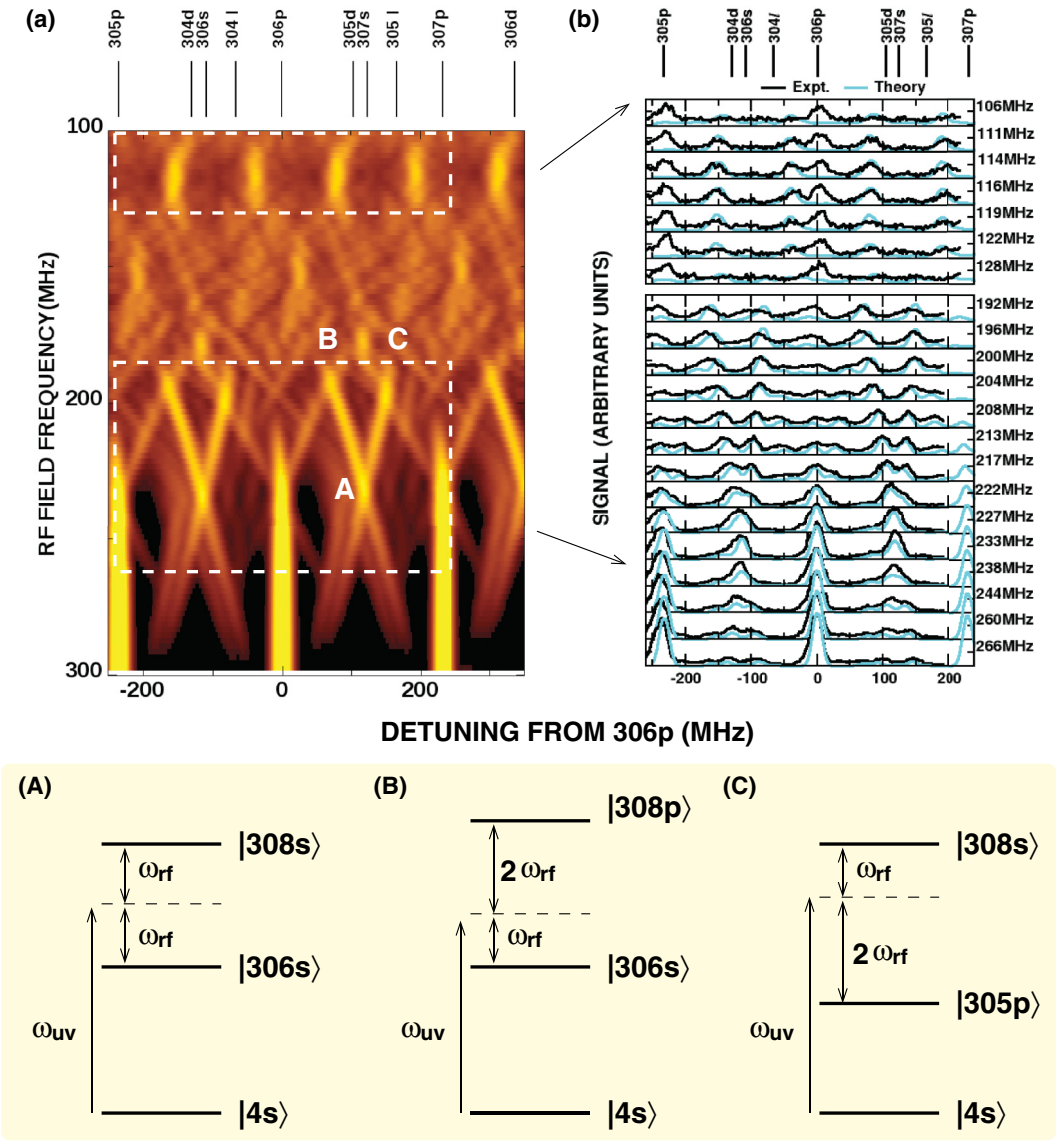

FIG. 8. (Color online) Evolution of the potassium photoexcitation spectrum in the vicinity of $n \sim 305$ as a function of the frequency of an rf drive field of amplitude $\sim$3 mV cm^{-1}. The excitation strengths are calculated, and the figure is arranged, as in Fig. 5. The processes responsible for excitation at the crossings labeled A, B, and C in (a) are shown schematically in the bottom frame (see text).

initially increases linearly with increasing field strength in qualitative agreement with the harmonic oscillator model. However, as the perturbation becomes stronger this linearity no longer holds and the excitation spectra become increasingly complex. The oscillator strength is distributed over many quasienergy levels due to the increasing importance of multiphoton processes that couple many Rydberg levels. The calculated spectra (Fig. 6) reproduce well the general behavior seen in the measured spectra, the small differences between the predicted and measured splittings of the spectral features being attributable, in part, to uncertainties in the rf drive field amplitude.

Additional insights can be obtained by considering how the photoexcitation spectra vary with $\omega_{\rm rf}$ for a fixed value of $F_{\rm rf}$. This is shown in Fig. 8 which compares excitation probabilities $\mathrm{Im}\chi(\omega_{\rm uv};\omega_{\rm rf},F_{\rm rf})$ to measured spectra. At high drive frequencies ($\omega_{\rm rf} > 250$ MHz) the excitation of p states is dominant. As the drive frequency is reduced and $|dF_{\rm rf}|$ becomes larger relative to δ in Eq. (11) the mixing between states becomes stronger allowing the excitation of s and d states. Since this requires absorption or emission of an rf photon, the positions of the excitation peaks vary linearly with $\omega_{\rm rf}$. For example, excitation of the 306s state will occur at a uv photon energy corresponding to $E_{306s} + \omega_{\rm rf}$ which involves emission of an rf photon as well as at a uv photon energy of $E_{306s} - \omega_{\rm rf}$ which requires absorption of an rf photon. In particular, the crossing (A) of the peaks seen for $\omega_{\rm rf} \simeq 230$ MHz at a detuning $\delta = 120$ MHz has contributions from both the 306s and 308s states even though the uv photon energy corresponds to that required for direct excitation of the 307s state. Similarly 304d and 306d states can be populated at the crossing. (The energy difference between 306s and 304d

or between 308s and 306d states is about 20 MHz, comparable to the effective experimental linewidth Δ.)

With further decreases in drive field frequency, multi-rf-photon processes become increasingly important. For example, near $\omega_{\rm rf} = 190$ MHz the Floquet states associated with the 306s and the 308s states cross with those corresponding to $E_{308p} - 2\omega_{\rm rf}$ (B) and $E_{305p} + 2\omega_{\rm rf}$ (C), respectively, for which excitation involves the emission or absorption of two rf photons. Since this is in a strongly coupled regime, the Floquet states associated with energies $E_{308p} - 2\omega_{\rm rf}$ or $E_{305p} + 2\omega_{\rm rf}$ are not pure 308p or 305p states. Numerical analysis indicates that these states are in fact a superposition of 307p and 309p states and 304p and 306p states, respectively, i.e., each comprises two p states coupled via a two-photon transition. Below $\omega_{\rm rf} \sim 180$ MHz many excitation peaks are visible whose positions change linearly with drive frequency. These features correspond to excitation processes that involve increasing numbers of rf photons, their number defining the slope of the linear variation in the peak position with rf drive frequency. While these multiphoton processes result in complex excitation spectra, the excitation probability is strongly suppressed at uv photon energies corresponding to the excitation of unperturbed p states. While this is reminiscent of EIT seen in few-level systems, here each Floquet state is a superposition involving many unperturbed states strongly coupled by the (near-resonant) drive field. As illustrated in Fig. 8, the calculated spectra reproduce well the behaviors seen in the measured spectra. However, peaks are seen in the data recorded at the lower rf drive frequencies at wavelengths corresponding to the energetic position of the unperturbed np states that are not present in the theoretical model employed.

V. SUMMARY AND OUTLOOK

The response of potassium high Rydberg states to an rf electric drive field has been investigated both experimentally and theoretically by probing the linear response, $\mathrm{Im}\chi(\omega_{\rm uv};\omega_{\rm rf},F_{\rm rf})$, to uv radiation. Even though high-n Rydberg states are close to the classical limit and the drive field is well removed from the optical regime, quantum optical features such as electromagnetically induced transparency (EIT), Autler-Townes splitting, and the Bloch-Siegert shift can be clearly identified even for comparatively weak drive fields. The photoexcitation spectra can be qualitatively understood with the help of a harmonic oscillator model exploiting the fact that the adjacent $ns - np$ and $np - (n+1)s$ spacings are nearly equal. With increasing drive field strength multiphoton transitions become ever more important and the photoexcitation spectra become more complex. The product states are superpositions of an increasing number of (unperturbed) states which is characteristic of behavior seen when the dynamics of a system become more classical.

In the current work $\mathrm{Im}\chi$ is determined by field ionization of the photoexcited Rydberg states. In the future it might also be possible to determine $\mathrm{Im}\chi$ by studying the absorption of the uv beam. Such optical measurement will be challenging due to the small oscillator strengths for the transitions involved but might be achieved using a high-density sample of trapped laser-cooled atoms. Future work might also include the addition of a propagating electromagnetic field to couple the ground hyperfine states whose frequency separation, ~461 MHz, matches that between levels with $\Delta n = 2$ transitions at $n \sim 305$. The combination of a purely electric field ($F_{\rm rf}$,$\omega_{\rm rf}$) with the electromagnetic field would allow for simultaneous, yet selective, coherent excitation of the hyperfine states in the 4s ground state and the Rydberg orbital degrees of freedom. This might then be used to manipulate and entangle nuclear, electronic, and photonic degrees of freedom, and would allow for unprecedented control of orbital and spin degrees of freedom. Nondestructive optical readout would, however, be crucial for implementing such protocols for quantum information storage and processing.

ACKNOWLEDGMENTS

Research was supported by the NSF under Grant No. 0964819, the Robert A. Welch Foundation under Grant No. C-0734, and by the FWF (Austria) under Grants No. SFB016 and No. P23359-N16. The Vienna Scientific Cluster was used for the calculations.

[1] L. S. Brown, Am. J. Phys. **41**, 525 (1973).
[2] A. Buchleitner, D. Delande, and J. Zakrzewski, Phys. Rep. **368**, 409 (2002).
[3] F. B. Dunning, J. J. Mestayer, C. O. Reinhold, S. Yoshida, and J. Burgdörfer, J. Phys. B **42**, 022001 (2009).
[4] F. B. Dunning, C. O. Reinhold, S. Yoshida, and J. Burgdörfer, Am. J. Phys. **78**, 796 (2010).
[5] M. Saffman, T. G. Walker, and K. Mølmer, Rev. Mod. Phys. **82**, 2313 (2010).
[6] R. Löw, H. Weimer, J. Nipper, J. B. Balewski, B. Butscher, H. P. Büchler, and T. Pfau, J. Phys. B **45**, 113001 (2012).
[7] S. H. Autler and C. H. Townes, Phys. Rev. **100**, 703 (1955).
[8] J. H. Shirley, Phys. Rev. B **138**, 979 (1965).
[9] M. Fleischhauer, A. Imamoglu, and J. P. Marangos, Rev. Mod. Phys. **77**, 633 (2005).
[10] A. K. Mohapatra, T. R. Jackson, and C. S. Adams, Phys. Rev. Lett. **98**, 113003 (2007).
[11] H. Schempp, G. Günter, C. S. Hofmann, C. Giese, S. D. Saliba, B. D. DePaola, T. Amthor, M. Weidemüller, S. Sevinçli, and T. Pohl, Phys. Rev. Lett. **104**, 173602 (2010).
[12] C. Ates, S. Sevinçli, and T. Pohl, Phys. Rev. A **83**, 041802 (2011).
[13] D. Petrosyan, J. Otterbach, and M. Fleischhauer, Phys. Rev. Lett. **107**, 213601 (2011).
[14] P. Ranitovic, X. M. Tong, C. W. Hogle, X. Zhou, Y. Liu, N. Toshima, M. M. Murnane, and H. C. Kapteyn, Phys. Rev. Lett. **106**, 193008 (2011).

[15] M. Tarana and C. H. Greene, Phys. Rev. A **85**, 013411 (2012).
[16] F. Bloch and A. Siegert, Phys. Rev. **57**, 522 (1940).
[17] C. L. Stokely, J. C. Lancaster, F. B. Dunning, D. G. Arbó, C. O. Reinhold, and J. Burgdörfer, Phys. Rev. A **67**, 013403 (2003).
[18] R. d. L. Kronig, J. Opt. Soc. Am. **12**, 547 (1926).
[19] H. A. Kramers, Phys. Z. **30**, 522 (1929).
[20] M. L. Zimmerman, M. G. Littman, M. M. Kash, and D. Kleppner, Phys. Rev. A **20**, 2251 (1979).
[21] N. B. Delone, S. P. Goreslavsky, and V. P. Krainov, J. Phys. B **27**, 4403 (1994).
[22] V. A. Davydkin and B. A. Zon, Opt. Spectrosc. **51**, 13 (1981).
[23] E. Jaynes and F. Cummings, Proc. IEEE **51**, 89 (1963).